ISIJ International, Vol. 57 (2017), No. 10, pp. 1725–1732

Activities of Fe_xO in Molten Slags Coexisting with Solid CaO and Ca_2SiO_4–$Ca_3P_2O_8$ Solid Solution

Kohei MIWA,[1] Ryota MATSUGI[2] and Masakatsu HASEGAWA[2]*

1) Graduate Student, Kyoto University. Now at Dowa Holdings Co., LTD., 4-14-1 Sotokanda, Chiyoda-ku, Tokyo, 101-0021 Japan.
2) Department of Energy Science and Technology, Kyoto University, Yoshida-honmachi, Sakyo-ku, Kyoto, 606-8501 Japan.

(*Received on April 6, 2017; accepted on August 9, 2017*)

In steelmaking processes, there are incentives to reduce slag volume and CaO consumption. The key to meet these requirements is the better understanding of CaO dissolution mechanism into molten slag, which relies on the knowledge of the thermochemical properties of slags and fluxes used for dephosphorization. In this study, the liquidus compositions coexisted with solid CaO and Ca_2SiO_4–$Ca_3P_2O_8$ solid solution simultaneously were determined in the quaternary system CaO–SiO_2–P_2O_5–Fe_xO at 1 573 K. Measurements were also conducted on the Fe_xO activities at temperatures between 1 542 K and 1 604 K by virtue of an electrochemical technique. By using the present experimental results, phosphorus distribution ratios were estimated.

KEY WORDS: dephosphorization; activity; di-calcium silicate; tri-calcium phosphate; solid solution.

1. Introduction

From the viewpoint of environmentally friendly steelmaking processes, there is a strong incentive to reduce slag volume. The key toward this end is a more effective utilization of CaO in removing phosphorus from hot metal, which can be expressed by

$$2\left[\mathrm{P}\right]_{\mathrm{Fe}} + 5\left(\mathrm{FeO}\right)_{\mathrm{slag}} = \left(\mathrm{P_2O_5}\right)_{\mathrm{slag}} + 5\left\{\mathrm{Fe}\right\} \quad \text{..... (1)}$$

$$\log K\left(1\right) = \log\left(a_{P_2O_5} / h_P^2\ a_{FeO}^5\right) = -15.48 + 5\,026 / \left(T / \mathrm{K}\right)^{1-4)} \quad \text{..... (2)}$$

a_i: activity of component i
h_i: Henrian activity of component i

In Eq. (1), $[P]_{Fe}$ is phosphorus in liquid iron, $(FeO)_{slag}$ and $(P_2O_5)_{slag}$ represent FeO and P_2O_5 in slag, respectively, and {Fe} is molten iron. It has been reported that P_2O_5 in slag reacts with CaO to form solid solution between di-calcium silicate, Ca_2SiO_4, and tri-calcium phosphate, $Ca_3P_2O_8$.[5]

Matsushima *et al*. determined the dissolution rate of solid CaO into liquid slag by measuring the decreasing rate of a diameter of a CaO cylinder dipped in CaO–SiO_2–FeO molten slag.[6] They concluded that the driving force of CaO dissolution was the difference between initial and equilibrium contents of CaO in molten slag saturated with Ca_2SiO_4. It has been also pointed out that Ca_2SiO_4 prevents dissolution of solid CaO into molten slag, because it is often formed on the surfaces of CaO particles, although Ca_2SiO_4–$Ca_3P_2O_8$ solid solution is an important phase in which P_2O_5 is condensed.

The reaction mechanism between solid CaO and CaO–SiO_2–P_2O_5–FeO molten slag has been reported by Hamano *et al*.[7] and Fukagai *et al*.,[8] as follows.
(a) Solid CaO dissolves into molten slag. CaO and SiO_2 are consumed due to the formation of Ca_2SiO_4. (**Fig. 1**(a))
(b) The FeO content in molten slag increases. According to the activity gradient of FeO, Fe^{2+} diffuses from FeO rich melt to both CaO and bulk slag. CaO–FeO layer is formed beside solid CaO. (Fig. 1(b))

Based on these foregoing comments, the present study aimed at determining the liquidus compositions and the Fe_xO activities in CaO–SiO_2–P_2O_5–Fe_xO quaternary heterogeneous slags containing solid CaO and Ca_2SiO_4–$Ca_3P_2O_8$ solid solution. Before discussing phase relations within this quaternary system of CaO–SiO_2–P_2O_5–Fe_xO, it seems to be pertinent to show the iso-thermal section of the ternary system CaO–SiO_2–P_2O_5 at 1 573 K.[9] As seen in **Fig. 2**(a), Ca_2SiO_4–$Ca_3P_2O_8$ solid solution can coexist with solid CaO. In this figure and hereafter, the following abbreviations are used.

C_2S = Ca_2SiO_4 = $2CaO{\cdot}SiO_2$
C_3P = $Ca_3P_2O_8$ = $3CaO{\cdot}P_2O_5$
<C_2S–C_3P>ss = solid solution between Ca_2SiO_4 and $Ca_3P_2O_8$
C_3S = Ca_3SiO_5 = $3CaO{\cdot}SiO_2$
CS = $CaSiO_3$ = $CaO{\cdot}SiO_2$
C_4P = $Ca_4P_2O_9$ = $4CaO{\cdot}P_2O_5$
L3: CaO–SiO_2–Fe_xO ternary liquid phase
L4: CaO–SiO_2–P_2O_5–Fe_xO quaternary liquid phase
$(mass\%\ i)_L$: concentration of component i in liquid slag
$(mass\%\ i)_{SS}$: concentration of component i in <C_2S–C_3P>ss

* Corresponding author: E-mail: hasegawa.masakatsu.7r@kyoto-u.ac.jp
DOI: http://dx.doi.org/10.2355/isijinternational.ISIJINT-2017-188

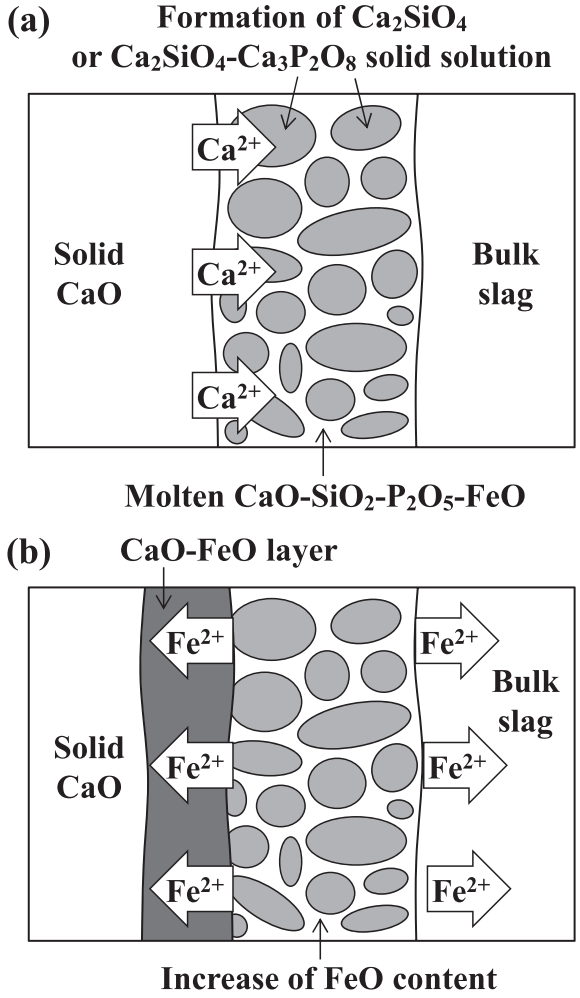

Fig. 1. Schematics of reaction mechanisms between solid CaO and molten slag.[7)]

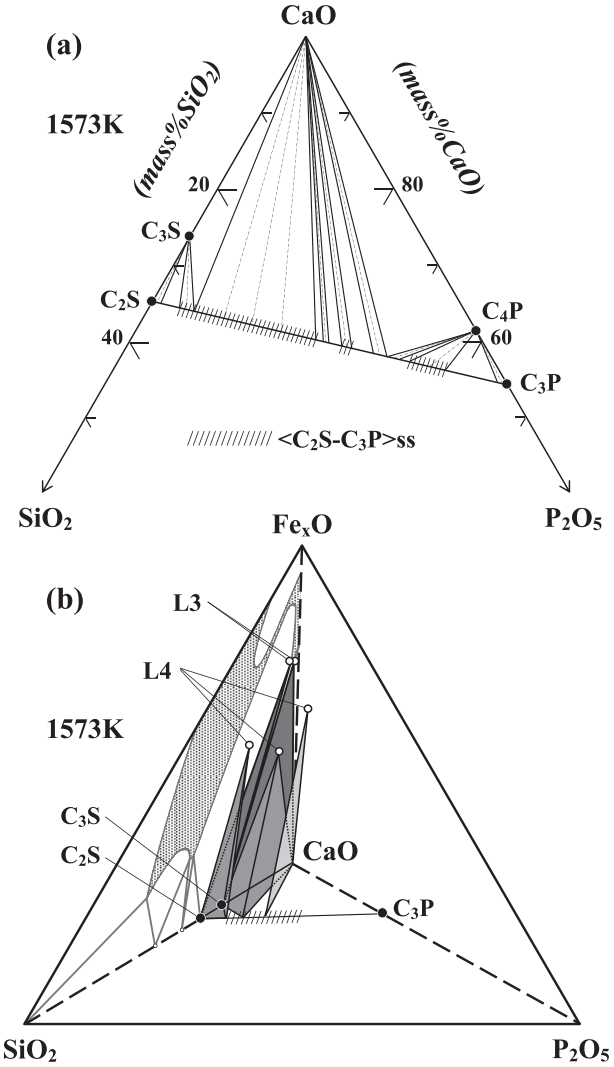

Fig. 2. (a) Iso-thermal section of the CaO–SiO_2–P_2O_5 ternary system at 1 573 K.[9)] (b) Schematic diagram of phase relationship in the CaO–SiO_2–P_2O_5–Fe_xO quaternary system at 1 573 K.

[*mass*% *i*]$_{Fe}$: concentration of component *i* in molten iron

When iron oxide is added to the ternary system of CaO–SiO_2–P_2O_5, Fe_xO would form quaternary liquid phase. Figure 2(b) schematically shows phase relations in the CaO–SiO_2–P_2O_5–Fe_xO quaternary system at 1 573 K; the base CaO–SiO_2–P_2O_5 and the side CaO–SiO_2–Fe_xO of this tetrahedron represent the phase diagrams of the corresponding ternary systems at 1 573 K,[9,10)] respectively. As the P_2O_5 content increases, the 3-phase coexistences of CaO + C_3S + L3 and C_3S + C_2S + L3 would change to the 4-phase coexistences of CaO + C_3S + <C_2S–C_3P>ss + L4 and C_3S + C_2S + <C_2S–C_3P>ss + L4, respectively,[11)] and then these two 4-phase regions would join to form the 3-phase region of CaO + <C_2S–C_3P>ss + L4. In the present study, the compositions of L4 coexisted with solid CaO and <C_2S–C_3P>ss simultaneously were determined by using electron probe micro analysis (EPMA), and, subsequently the activities of Fe_xO in the 3-phase region of CaO + <C_2S–C_3P>ss + L4 were determined by employing an electrochemical technique incorporating magnesia stabilized zirconia.

2. Experimental Aspects

2.1. EPMA Studies

The experimental apparatus is schematically shown in **Fig. 3**, and starting materials used for phase equilibrium study are listed in **Table 1**. The compounds listed in this table were mixed with iron oxide, and pressed into a steel die. The bulk compositions of the oxide mixtures are given in **Table 2**. As shown in Fig. 3(b), oxide pellets were charged in an iron crucible with powdery oxide of the same bulk composition as pellets, in order to facilitate removing pellets from a crucible after heating. Oxide samples were held at 1 573 K over 48 hours under a stream of purified argon to yield the appropriate 3-phase region. The gas purification train consisted of silica-gel, phosphorus pentoxide and magnesium chips held at 823 K. By pushing down a magnesia crucible, a plastic plate was broken, and then samples were quenched in liquid nitrogen. The resulting samples were submitted, firstly, to X-ray diffraction analysis to confirm the expected solid compounds, and, subsequently, to EPMA to determine the compositions of quaternary liquid phase and <C_2S–C_3P>ss.

2.2. Electrochemical Measurements

The slags under considerations were prepared by mixing CaO, <C_2S–C_3P>ss and iron oxide; the bulk compositions

of slags are summarized in **Table 3**. The experimental setup was schematically shown in **Fig. 4**. An iron crucible was charged with 3 to 6 g of slag and about 35 g of pure silver. The crucible was then heated to the experimental temperature under a stream of purified argon inside a SiC resistance furnace.

As shown in Fig. 4, the oxygen sensor consisted of a zirconia tube closed at one end and a two-phase mixture of Mo + MoO_2 as the reference electrode. The zirconia tubes used in this study were stabilized by 9 mol% of MgO, and supplied by Nikkato Corp., Japan, and these tubes had an inner diameter of 4 mm, an outer diameter of 6 mm and a length of 50 mm. A molybdenum rod of 3 mm diameter was used as an electric conductor to the reference electrode, while the electrical contact to the outer electrode of the zirconia probe was made by the liquid silver and a steel rod soldered to the iron crucible. The zirconia tubes used in this study has a satisfactory resistance to the FeO-containing slags.

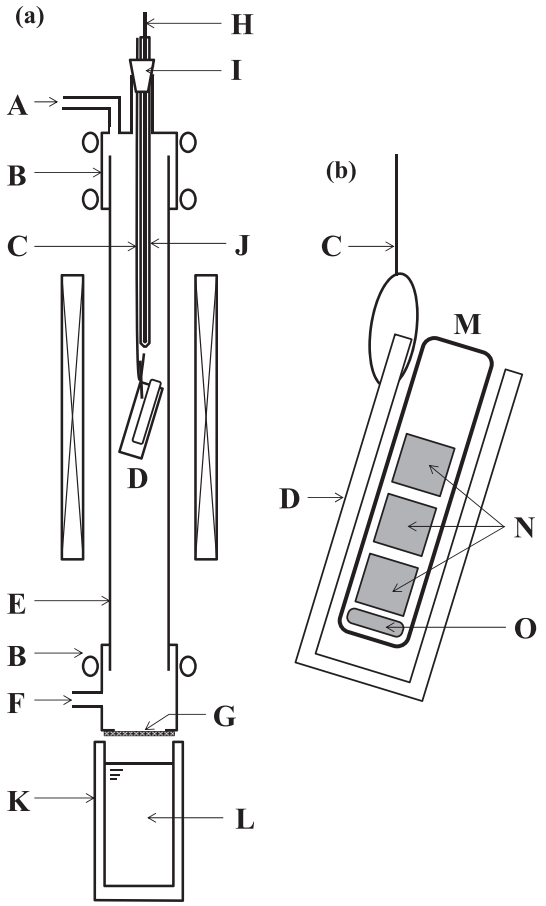

Fig. 3. Experimental apparatus used for phase equilibrium study. (A) Gas outlet, (B) Water-cooled brass flange, (C) Molybdenum rod, (D) Magnesia crucible, (E) Mullite reaction tube, (F) Gas inlet, (G) Plastic plate, (H) Pt-PtRh13 thermocouple, (I) Robber stopper, (J) Alumina sheath, (K) Thermos bottle, (L) Liquid nitrogen, (M) Iron crucible, (N) Oxide pellets, (O) powdery oxide.

Values for the open-circuit electromotive forces (*emf*) of the oxygen probes were read with a digital voltmeter of 100 MΩ input resistance with an accuracy of ± 0.01 mV. *Emf* readings were continued until stable cell potentials were obtainable, and the reproducibilities of cell potentials were confirmed by temperature cycling. Temperatures were measured with a Pt-PtRh13 thermocouple and controlled to ± 1 K by using a control thermocouple and PID-type temperature regulator.

The open-circuit electromotive force, E, of the cell is given by[12)]

$$E = \frac{RT}{F} \ln \frac{P_{O_2}\left(ref.\right)^{1/4} + P_e^{1/4}}{P_{O_2}^{1/4} + P_e^{1/4}} + E_t \quad \text{..... (3)}$$

, where R is the gas constant, T is temperature, F is the Faraday constant, E_t is thermo-*emf* between Mo (positive) and Fe (negative), and P_e is the oxygen partial pressure at which the ionic and the n-type electronic conductivities are equal. Values for E_t and P_e used in this study have been reported as follows, respectively.

$$E_t \,/\,\mathrm{mV} = -14.69 + 0.0227\left(T\,/\,\mathrm{K}\right) \text{[13)]} \quad \text{..... (4)}$$

$$\log\left(P_e\,/\,\mathrm{atm}\right) = +20.40 - 6.45\times10^4\,/\left(T\,/\,\mathrm{K}\right) \text{[14)]} \quad \text{..... (5)}$$

The oxygen partial pressure at the reference electrode, $P_{O_2}\left(ref.\right)$, was given by

$$\log\left[P_{O_2}\left(ref.\right)/\,\mathrm{atm}\right] = +8.84 - 30\,100\,/\left(T\,/\,\mathrm{K}\right) \text{[15)]} \quad \text{... (6)}$$

When the standard state for Fe_xO was taken as pure non-stoichiometric liquid Fe_xO in equilibrium with pure solid Fe, the activities of Fe_xO could be calculated by

$$a_{Fe_xO} = \left(\frac{P_{O_2}}{P_{O_2}^{\circ}}\right)^{1/2} \quad \text{..... (7)}$$

, where $P_{O_2}^{\circ}$ is the equilibrium oxygen partial pressure of the mixture of pure solid Fe + pure liquid Fe_xO, as given by the following formula.

$$\log\left[P_{O_2}^{\circ}\,/\,\mathrm{atm}\right] = +4.39 - 2.35\times10^4\,/\left(T\,/\,\mathrm{K}\right) \text{[2)]} \quad \text{..... (8)}$$

Table 1. Starting materials used for phase equilibrium study.

Compound	Preparation
$CaCO_3$	Obtained from Nacalai Tesque, Inc., Kyoto, Japan, and dried at 413 K.
SiO_2	Obtained from Nacalai Tesque, Inc., Kyoto, Japan, and dried at 413 K.
C_3P	Obtained from Nacalai Tesque, Inc., Kyoto, Japan, and dried at 413 K.
CaO	$CaCO_3$ heated at 1 273 K for 2 hours.
C_2S	$CaCO_3$ mixed with SiO_2, and fired at 1 573 K for 24 hours.
$<C_2S–C_3P>$ss	C_3P mixed with C_2S, and fired at 1 573 K for 24 hours.

Table 2. Bulk and equilibrium compositions of the three-phase assemblages at 1 573 K.

Bulk composition (mass%)				Phase	Equilibrium composition (mass%)					$\log L_P^{SS/L}$
CaO	SiO_2	P_2O_5	Fe_xO		CaO	SiO_2	P_2O_5	Fe_xO	$(mass\%C_3P)_{SS}$	
				CaO	87.44	0.61	0.15	11.81	–	
71.02	9.55	2.75	16.68	<C_2S–C_3P>ss	60.61	28.72	8.38	2.29	18	1.398
				L4	30.10	1.31	0.34	68.27	–	
				CaO	88.15	0.72	0.29	10.84	–	
70.84	8.83	3.66	16.67	<C_2S–C_3P>ss	60.31	26.33	11.19	2.16	24	1.319
				L4	30.25	0.87	0.39	68.50	–	
				CaO	86.50	0.59	0.23	12.68	–	
70.60	8.02	4.73	16.65	<C_2S–C_3P>ss	61.28	23.02	13.56	2.14	31	1.463
				L4	27.72	1.21	0.65	70.43	–	

Table 3. Bulk compositions of slags used for measurements of Fe_xO activities.

Bulk composition (mass%)				Remark
CaO	SiO_2	P_2O_5	Fe_xO	$(mass\%C_3P)_{SS}$
79.39	9.54	2.75	8.33	18
79.17	8.84	3.66	8.33	24
78.92	8.02	4.73	8.33	31

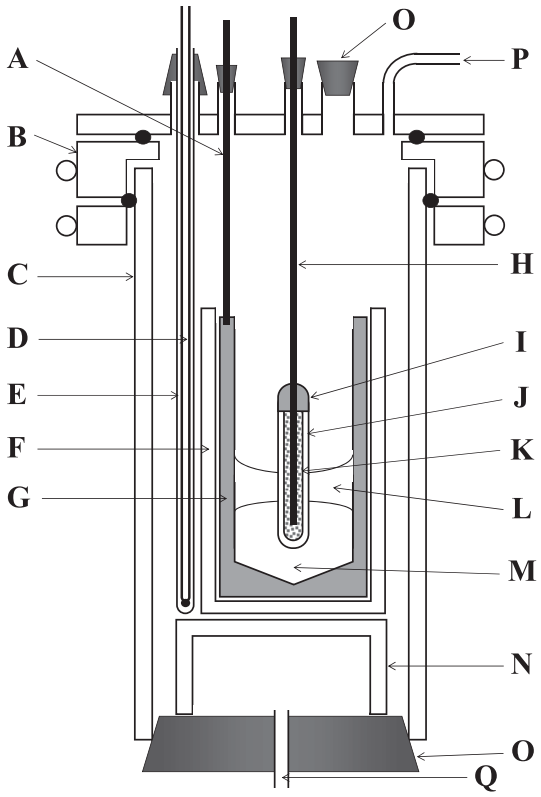

Fig. 4. Experimental apparatus used for activity measurements. (A) Iron rod, (B) Water-cooled brass flange, (C) Mullite reaction tube, (D) Pt-PtRh13 thermocouple, (E) Alumina sheath, (F) Alumina crucible, (G) Iron crucible, (H) Molybdenum rod, (I) Zirconia cement, (J) ZrO_2(MgO) solid electrolyte tube, (K) Mo + MoO_2 reference electrode, (L) Slag, (M) Liquid silver, (N) Alumina pedestal, (O) Rubber stopper, (P) Gas inlet, (Q) Gas outlet.

3. Experimental Results and Discussion

3.1. EPMA Studies

XRD and EPMA studies confirmed that all the slags investigated in this study occurred at the expected 3-phase region of CaO + <C_2S–C_3P>ss + L4, and the compositions are numerically given in Table 2.

Figure 5 shows the present values for the contents of Fe_xO, SiO_2 and P_2O_5 in the quaternary liquid slags plotted against the C_3P content in <C_2S–C_3P>ss, together with the literature data for the 3-phase regions of CaO + C_3S + L3 and C_3S + C_2S + L3 in the CaO–SiO_2–Fe_xO ternary system[10] and the 4-phase regions of CaO + C_3S + <C_2S–C_3P>ss + L4 and C_3S + C_2S + <C_2S–C_3P>ss + L4 in the CaO–SiO_2–P_2O_5–Fe_xO quaternary system.[11] The Fe_xO content decreased as the C_3P content increased up to 12 mass%, and then it increased, but it was almost constant in the 3-phase region of CaO + <C_2S–C_3P>ss + L4. The concentrations of SiO_2 and P_2O_5 were very low in the composition range investigated. Based on these results, the liquid phase coexisted with CaO and <C_2S–C_3P>ss simultaneously could be considered to be CaO–Fe_xO binary melt approximately.

The compositions of molten slags equilibrated with <C_2S–C_3P>ss, in which $(mass\%P_2O_5)_{SS}$ were lower than 5, have been reported in the literature. In **Fig. 6**, the present results are projected onto the pseudo-ternary field of CaO–(SiO_2+P_2O_5)–Fe_xO at 1 573 K, together with the literature data.[16,17] The 3-phase region of CaO + <C_2S–C_3P>ss + L4 and the liquidus lines coexisted with <C_2S–C_3P>ss could be illustrated in this diagram. As mentioned above, the liquidus compositions in the 3-phase region investigated in this study were insensitive to the variation of $(mass\%C_3P)_{SS}$. The liquidus line saturated with <C_2S–C_3P>ss, however, should depend on $(mass\%C_3P)_{SS}$; this would be future work.

Next, consider the phosphorus distribution ratio along the liquidus line saturated with <C_2S–C_3P>ss seen in Fig. 6. For effective dephosphorization, P_2O_5 in slag should be condensed in solid phases. The distribution ratio of P_2O_5 between solid and liquid phases was defined by

$$L_P^{SS/L} = \frac{(mass\%P_2O_5)_{SS}}{(mass\%P_2O_5)_L} \quad \text{..... (9)}$$

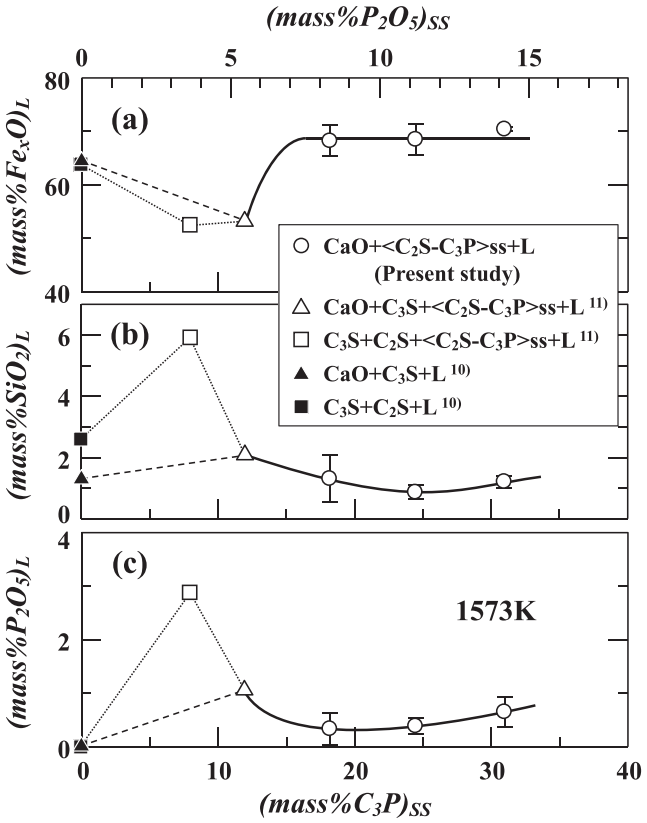

Fig. 5. Liquidus compositions plotted against the C_3P content in C_2S–C_3P solid solution at 1 573 K. (a) Fe_xO, (b) SiO_2, (C) P_2O_5.

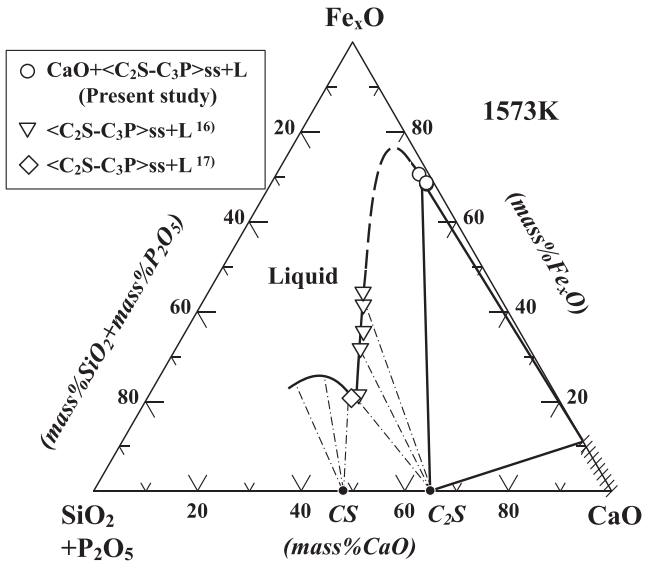

Fig. 6. Phase relationship projected on the CaO–(SiO_2+P_2O_5)–Fe_xO pseudo-ternary field at 1 573 K.

Table 2 gives the values for $L_P^{SS/L}$ of the heterogeneous slags investigated in this study, and **Fig. 7** shows $L_P^{SS/L}$ plotted against $(mass\%Fe_xO)_L$. It has been reported that the relationship between logarithmic value for $L_P^{SS/L}$ and $(mass\%Fe_xO)_L$ would be linear and scarcely dependent on temperature.[17–19] As seen in this figure, the present results were in very good agreement with the literature data.

3.2. Electrochemical Measurements

In this study, the Fe_xO activities were determined in the 3-phase region of CaO + <C_2S–C_3P>ss + L4. **Tables 4**, **5** and **6** give the experimental results obtained when $(mass\%C_3P)_{SS}$ are 18, 24 and 31, respectively, and the present values for $\log a_{Fe_xO}$ are shown in **Fig. 8** as functions of reciprocal temperature. By using the least squares method, the present values for could be well expressed by the following formulae;

$$\log a_{Fe_xO} = 0.418 - \frac{1\,075}{(T/\mathrm{K})} \pm 0.009 \quad (mass\%C_3P)_{SS} = 18 \qquad \text{.....(10)}$$

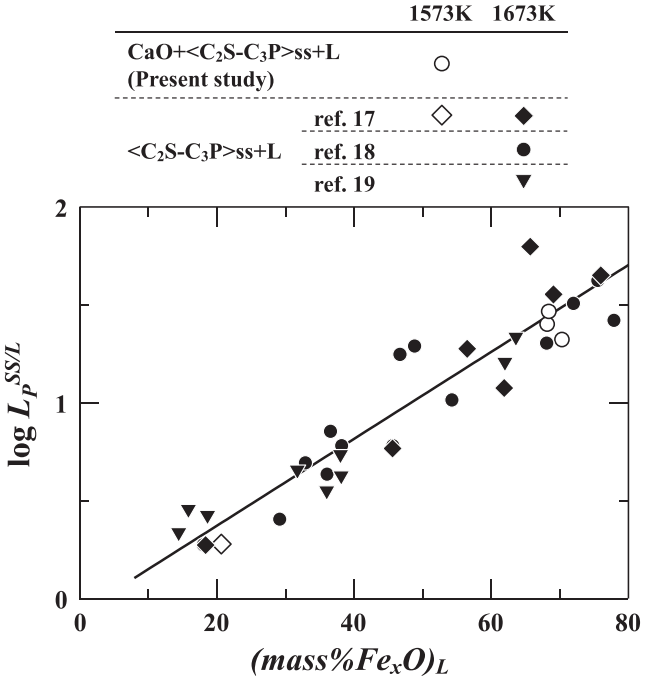

Fig. 7. P_2O_5 distribution ratio between solid solution and liquid slag plotted against Fe_xO content in liquid slag.

Table 4. Experimental results for activity measurements; $(mass\%C_3P)_{SS}$=18.

No.	T/K	E/mV	$\log(P_{O_2}/\mathrm{atm})$	$\log a_{Fe_xO}$
7-3	1 552	76.49 ± 0.10	−11.28	−0.264
7-4	1 563	78.82 ± 0.08	−11.17	−0.260
7-8	1 543	76.94 ± 0.04	−11.41	−0.283
7-10	1 545	74.56 ± 0.05	−11.35	−0.264
8-1	1 577	83.85 ± 0.03	−11.05	−0.269
8-2	1 591	86.61 ± 0.06	−10.91	−0.262
8-3	1 552	79.45 ± 0.04	−11.32	−0.284
8-4	1 563	81.38 ± 0.02	−11.20	−0.277
8-5	1 583	84.99 ± 0.06	−10.99	−0.266
8-6	1 603	88.75 ± 0.08	−10.78	−0.256
8-7	1 573	82.42 ± 0.11	−11.08	−0.266
8-8	1 543	76.95 ± 0.04	−11.41	−0.283
8-9	1 563	80.22 ± 0.06	−11.18	−0.269
8-11	1 552	80.79 ± 0.10	−11.34	−0.292
8-12	1 573	76.98 ± 0.02	−11.01	−0.231

Table 5. Experimental results for activity measurements; $(mass\%C_3P)_{SS}$=24.

No.	T/K	E/mV	$\log(P_{O_2}/\mathrm{atm})$	$\log a_{Fe_xO}$
5-1	1 575	86.35 ± 0.08	−11.11	−0.288
5-3	1 595	85.58 ± 0.12	−10.84	−0.249
5-4	1 552	75.64 ± 0.12	−11.27	−0.259
5-5	1 583	83.21 ± 0.09	−10.96	−0.254
5-9	1 603	87.61 ± 0.08	−10.77	−0.249
6-1	1 576	83.77 ± 0.11	−11.06	−0.270
6-2	1 593	88.85 ± 0.12	−10.91	−0.273
6-3	1 552	79.07 ± 0.06	−11.31	−0.281
6-4	1 582	86.45 ± 0.06	−11.02	−0.277
6-7	1 574	84.54 ± 0.13	−11.10	−0.278
6-8	1 583	87.02 ± 0.12	−11.01	−0.279
6-9	1 583	85.11 ± 0.12	−10.99	−0.267
6-10	1 552	78.33 ± 0.11	−11.30	−0.276
6-11	1 544	75.05 ± 0.06	−11.37	−0.269
6-12	1 564	79.51 ± 0.11	−11.16	−0.263
6-15	1 572	81.37 ± 0.09	−11.08	−0.261
6-16	1 603	93.46 ± 0.13	−10.84	−0.286
6-17	1 562	79.80 ± 0.11	−11.19	−0.268
6-18	1 551	76.15 ± 0.08	−11.29	−0.264
6-20	1 592	91.09 ± 0.08	−10.95	−0.289
6-21	1 573	84.01 ± 0.08	−11.10	−0.277
6-22	1 542	73.58 ± 0.08	−11.38	−0.263
6-23	1 542	73.42 ± 0.06	−11.37	−0.262
6-24	1 553	75.47 ± 0.07	−11.25	−0.256
6-25	1 573	83.63 ± 0.06	−11.10	−0.274

$$\log a_{Fe_xO} = -0.393 + \frac{195}{(T/\mathrm{K})} \pm 0.009 \quad (mass\%C_3P)_{SS} = 24 \qquad \text{..... (11)}$$

$$\log a_{Fe_xO} = 0.493 - \frac{1\,211}{(T/\mathrm{K})} \pm 0.022 \quad (mass\%C_3P)_{SS} = 31 \qquad \text{..... (12)}$$

Figure 9(a) shows the Fe_xO activities at 1 573 K plotted against $(mass\%C_3P)_{SS}$, in comparison with the literature data.[11,20] The Fe_xO activity had a minimum in the 4-phase regions CaO + C_3S + <C_2S–C_3P>ss + L4 or C_3S + C_2S + <C_2S–C_3P>ss + L4, and was almost constant in the 3-phase region of CaO + <C_2S–C_3P>ss + L4; such behaviors were consistent with those of Fe_xO content in liquid phase, seen in Fig. 5(a).

As already mentioned, it has been reported that, in the reaction between solid CaO and CaO–SiO_2–P_2O_5–Fe_xO molten slag, CaO–Fe_xO layer is formed beside solid CaO due to the activity gradient of Fe_xO.[7] (Fig. 1(b)) Hamano *et al*. noted that the Fe_xO activities at 1 573 K in Fe_xO rich melt saturated with C_2S and bulk slag could be calculated to be 0.85 and 0.27, respectively,[7] by using the regular solution model.[21] Based on the present experimental results, CaO–Fe_xO layer would correspond to the liquid phase coexisted with solid CaO and <C_2S–C_3P>ss simultaneously, in which the Fe_xO activity at 1 573 K was determined to be 0.53–0.54 in this study. Consequently, it could be concluded that the Fe_xO activity for CaO–Fe_xO liquid phase was lower than that for Fe_xO rich melt saturated with C_2S; this was not inconsistent with the dissolution mechanism of solid CaO into molten slag.[7,8]

Table 6. Experimental results for activity measurements; $(mass\%C_3P)_{SS}$=31.

No.	T/K	E/mV	$\log(P_{O_2}/\mathrm{atm})$	$\log a_{Fe_xO}$
1-1	1 573	87.86 ± 0.03	−11.15	−0.301
1-2	1 595	90.80 ± 0.02	−10.91	−0.282
1-3	1 544	81.66 ± 0.05	−11.45	−0.312
1-4	1 559	84.51 ± 0.05	−11.29	−0.304
1-5	1 584	88.46 ± 0.10	−11.02	−0.286
2-1	1 573	81.93 ± 0.02	−11.08	−0.263
2-2	1 593	96.32 ± 0.08	−11.00	−0.321
2-3	1 583	85.72 ± 0.04	−11.00	−0.270
2-4	1 542	75.78 ± 0.09	−11.40	−0.277
2-6	1 572	89.86 ± 0.05	−11.19	−0.316
3-2	1 551	94.95 ± 0.08	−11.53	−0.386
3-8	1 562	85.04 ± 0.07	−11.26	−0.302
3-9	1 551	81.92 ± 0.12	−11.36	−0.302
3-10	1 542	79.54 ± 0.08	−11.45	−0.302
3-11	1 573	81.23 ± 0.08	−11.07	−0.259
3-14	1 604	93.27 ± 0.12	−10.83	−0.283
3-15	1 554	82.21 ± 0.07	−11.33	−0.298
3-17	1 594	87.09 ± 0.10	−10.87	−0.260
3-18	1 574	84.92 ± 0.08	−11.10	−0.281
3-19	1 542	71.80 ± 0.08	−11.35	−0.251
4-1	1 570	81.22 ± 0.10	−11.11	−0.264
4-2	1 570	81.16 ± 0.10	−11.11	−0.263
4-3	1 591	86.17 ± 0.08	−10.90	−0.260
4-4	1 591	83.83 ± 0.06	−10.87	−0.245
4-5	1 553	83.69 ± 0.13	−11.36	−0.309
4-6	1 553	75.86 ± 0.05	−11.26	−0.259
4-7	1 589	83.56 ± 0.06	−10.89	−0.246
4-8	1 589	82.20 ± 0.03	−10.87	−0.238
4-9	1 574	84.82 ± 0.06	−11.10	−0.280
4-10	1 574	84.36 ± 0.10	−11.09	−0.277
4-11	1 543	74.79 ± 0.10	−11.38	−0.269
4-12	1 543	74.43 ± 0.10	−11.37	−0.267
4-13	1 543	73.00 ± 0.06	−11.35	−0.257
4-14	1 584	78.75 ± 0.04	−10.89	−0.224
4-15	1 584	83.62 ± 0.05	−10.96	−0.255
4-16	1 584	82.92 ± 0.03	−10.95	−0.251

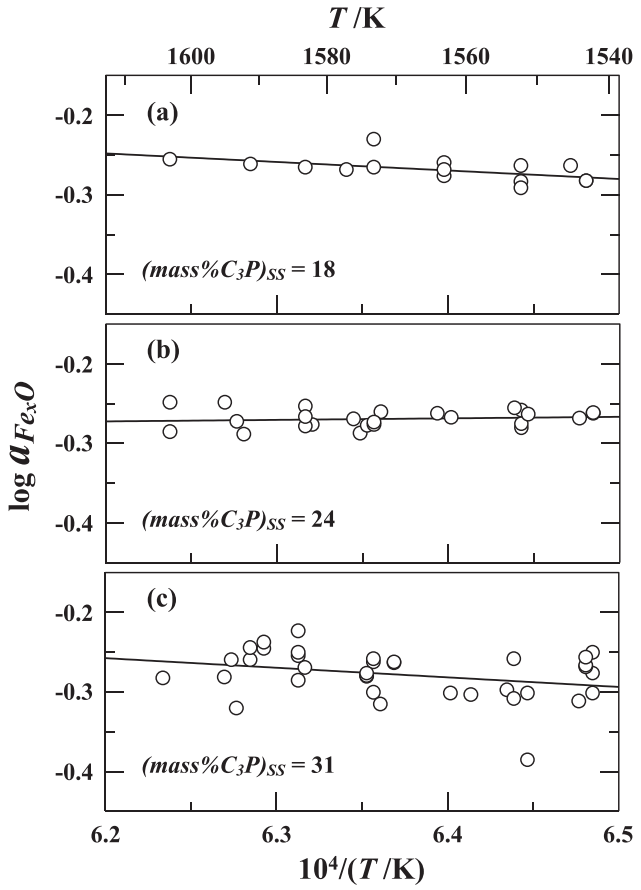

Fig. 8. Relation between logarithmic value for Fe_xO activity and reciprocal temperature.

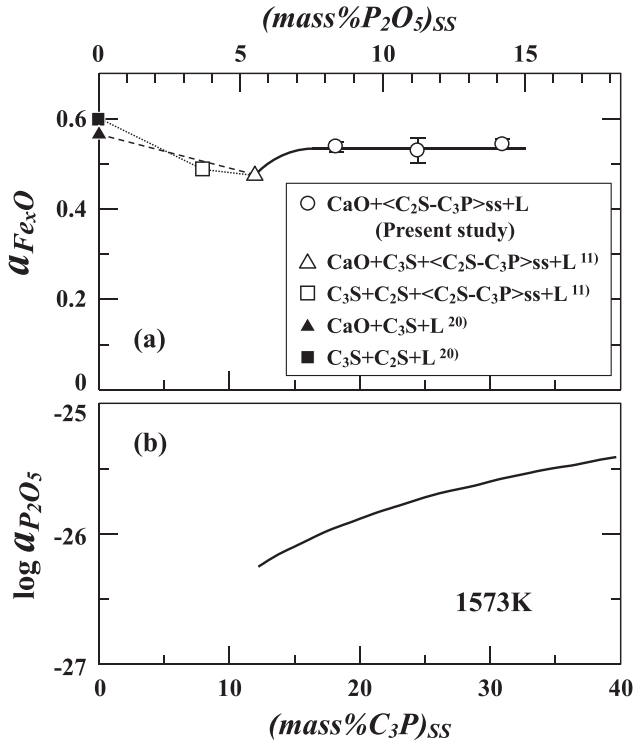

Fig. 9. Relation between the activity and the C_3P content in C_2S–C_3P solid solution at 1 573 K. (a) Fe_xO, (b) P_2O_5.

3.3. Phosphorus Distribution Ratio between Liquid Slag and Molten Iron

By the present authors, the C_3P activity in $<C_2S$–$C_3P>$ss at 1 573 K has been formulated as[22)]

$$\log a_{C_3P} = 6.80\times10^{-3} + 2\log Y + 3.81\times10^{-1}\times(1-Y)^2 \quad \text{... (13)}$$

, where Y represents the substitution ratio and is defined by

$$Y = 2\,n_{C_3P} / \left(n_{C_2S} + 2\,n_{C_3P}\right) \quad \text{..... (14)}$$

In Eq. (14), n_i denotes the number of moles of component i in solid solutions. As seen in Table 2, $(mass\%Fe_xO)_{SS}$ was less than 2.5 in the 3-phase region of CaO + $<C_2S$–$C_3P>$ss + L4. Therefore, it was assumed that the C_3P activity in the 3-phase region under consideration was identical to that calculated by Eq. (13). Furthermore, based on the assumption that the CaO activity was unity in this 3-phase region, the P_2O_5 activity could be derived by the following reaction, which represented the formation of C_3P from CaO and P_2O_5.

$$3CaO + P_2O_5 = C_3P \quad \text{..... (15)}$$

$$\log K(23) = \log a_{C_3P} - 3\log a_{CaO} - \log a_{P_2O_5} = 24.80 \text{ at } 1\,573\text{ K}^{1,23,24)} \quad \text{..... (16)}$$

$$\log a_{P_2O_5} = \log a_{C_3P} - 24.80 = -24.79 + 2\log Y + 3.81\times10^{-1}\times(1-Y)^2 \quad \text{... (17)}$$

Figure 9(b) shows the P_2O_5 activity at 1 573 K calculated from Eq. (17). In the 3-phase region of CaO + $<C_2S$–$C_3P>$ss + L4, the P_2O_5 activity increased with an increase in $(mass\%C_3P)_{SS}$.

Now, consider the distribution ratio of phosphorus between liquid slag and molten iron, defined by

$$L_P^{L/Fe} = \frac{(mass\%P)_L}{[mass\%P]_{Fe}} \quad \text{..... (18)}$$

For carbon-saturated {Fe–C–P} liquid alloys, the Henrian activity of phosphorus is expressed by

$$\log h_P = \log[mass\%P]_{Fe} + e_P^C[mass\%C]_{Fe} + e_P^P[mass\%P]_{Fe} \quad \text{..... (19)}$$

, where e_i^j represents the first order interaction coefficient

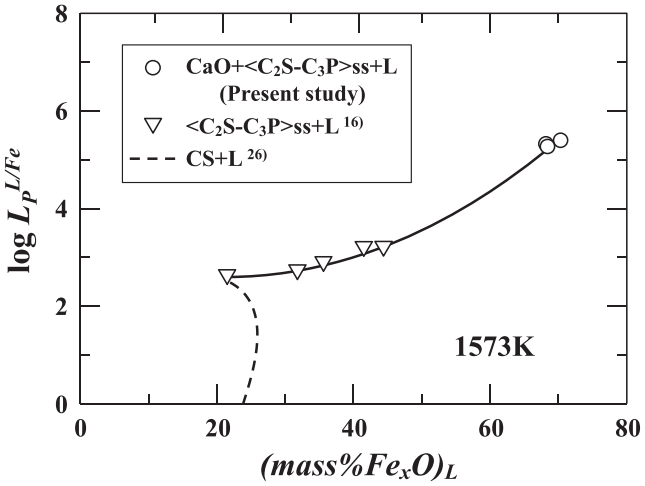

Fig. 10. Phosphorus distribution ratio between liquid slag and molten iron plotted against Fe_xO content in liquid slag.

in liquid iron[4,25] and $[mass\%C]_{Fe}$ is the carbon concentration in liquid iron saturated with solid carbon. Eqs. (2), (18) and (19) imply that $L_P^{L/Fe}$ for the 3-phase region of CaO + $<C_2S–C_3P>$ss + L4 can be calculated by using the Fe_xO activities (Eqs. (10), (11) and (12)), the P_2O_5 activity (Eq. (17)) and the phosphorus content in liquid slag (Table 2). The calculation results are shown in **Fig. 10**, together with the literature data at 1 573 K.[16,26] By applying Le Chatelier's principle to Reaction (1), the thermochemical conditions to achieve high $L_P^{L/Fe}$ are high Fe_xO activity and low P_2O_5 activity (high basicity). The variations of $L_P^{L/Fe}$ along the liquidus lines coexisted with $<C_2S–C_3P>$ss and CS illustrated in Fig. 10 were consistent with these conditions and the phase relations in Fig. 6. It should be noted here that the values for $L_P^{L/Fe}$ in Fig. 10 were estimated by assuming that the oxygen potential was fixed by the equilibrium between Fe_xO in slag and metallic iron, in order to compare the present values with those reported in the literature at temperature below the melting point of pure iron.

4. Conclusion

In this study, attention was focused on the 3-phase assemblage of CaO + Ca_2SiO_4–$Ca_3P_2O_8$ solid solution + liquid slag in the quaternary system CaO–SiO_2–P_2O_5–Fe_xO. The liquidus compositions of this 3-phase region at 1 573 K were determined by employing EMPA. The contents of SiO_2 and P_2O_5 were very low in these quaternary liquid slags. The Fe_xO activities were also measured by using an electrochemical technique involving stabilized zirconia electrolyte. The present results were consistent with the reaction mechanism between solid CaO and molten slag. Based on the present experimental data, phosphorus distribution ratios were estimated.

Acknowledgment

This work was supported by ISIJ, the 19th Committee on Steelmaking of JSPS, and JSPS KAKENHI Grant Number 15K06524. These are gratefully acknowledged.

REFERENCES

1) E. T. Turkdogan and J. Pearson: *J. Iron Steel Inst.*, **175** (1953), 393.
2) M. Iwase, N. Yamada, K. Nishida and E. Ichise: *Trans. Iron Steel Soc. AIME*, **4** (1984), 69.
3) O. Kubaschewski, C. B. Alcock and P. J. Spencer: Materials Thermochemistry, 6th Ed., Pergamon Press, Oxford, (1993), 257.
4) G. K. Sigworth and J. F. Elliott: *Met. Sci.*, **8** (1974), 298.
5) H. Suito, Y. Hayashida and Y. Takahashi: *Tetsu-to-Hagané*, **63** (1977), 1252.
6) M. Matsushima, S. Yadoomaru, K. Mori and Y. Kawai: *Tetsu-to-Hagané*, **62** (1976), 182.
7) T. Hamano, S. Fukagai and F. Tsukihashi: *ISIJ Int.*, **46** (2006), 490.
8) S. Fukagai, T. Hamano and F. Tsukihashi: *ISIJ Int.*, **47** (2007), 187.
9) M. Matsu-sue, M. Hasegawa, K. Fushi-tani and M. Iwase: *Steel Res. Int*., **78** (2007), 465.
10) A. Muan and E. F. Osborn: Phase Equilibria among Oxides in Steelmaking, Addison-Wesley Publishing Company, Massachusetts, (1965), 113.
11) M. Hasegawa and M. Iwase: *Tetsu-to-Hagané*, **95** (2009), 222.
12) H. Schmalzried: *Z. Elektrochem.*, **66** (1962), 572.
13) M. Iwase, N. Yamada, E. Ichise and H. Akizuki: *Trans. Iron Steel Soc. AIME*, **5** (1984), 53.
14) M. Iwase, E. Ichise, T. Yamasaki and M. Takeuchi: *Trans. Jpn. Inst. Met*., **25** (1984), 43.
15) M. Iwase, M. Yasuda and T. Mori: *Electrochim. Acta*, **19** (1979), 261.
16) K. Ito and N. Sano: *Tetsu-to-Hagané*, **69** (1983), 1746.
17) R. Inoue and H. Suito: *ISIJ Int.*, **46** (2006), 174.
18) K. Ito, M. Yanagisawa and N. Sano: *Tetsu-to-Hagané*, **68** (1982), 342.
19) K. Shimauchi, S. Kitamura and H. Shibata: *Tetsu-to-Hagané*, **95** (2009), 229.
20) K. Takeuchi, T. Enaka, N. Kon-no, T. Hosotani, T. Orimoto and M. Iwase: *Steel Res.*, **68** (1997), 516.
21) S. Ban-ya: *ISIJ Int.*, **33** (1993), 2.
22) M. Hasegawa, Y. Kashiwaya and M. Iwase: *High Temp. Mater. Process*., **31** (2012), 421.
23) H. Yama-zoye, E. Ichise, H. Fujiwara and M. Iwase: *Trans. Iron Steel Soc. AIME*, **13** (1992), 41.
24) M. Iwase, N. Yamada, H. Akizuki and E. Ichise: *Arch. Eisenhuttenwes*., **55** (1984), 471.
25) H. Schenck and E. Steinmetz: Wirkungsparameter von Begleitelementen flüssiger Eisenlösungen und ihre gegenseitigen Beziehungen, 2erg. Aufl. Stahleisen Sonderberichte Hef, 7 (1968), 1.
26) J. Im, K. Morita and N. Sano: *ISIJ Int*., **36** (1996), 517.